PDIA3 Reduce Glioma-associated Macrophage/microglia Pro-tumor Activation trough IL-6-STAT3-PDIA3 Pathway.

Marta Chiavari
Universita Cattolica del Sacro Cuore
Gabriella Maria Pia Ciotti
Universita Cattolica del Sacro Cuore
Francesco Canonico
Policlinico Universitario Agostino Gemelli
Fabio Altieri
Universita degli Studi di Roma La Sapienza Dipartimento di scienze biochimiche
Pierluigi Navarra
Universita Cattolica del Sacro Cuore
Lucia Lisi (lucia.lisi@unicatt.it)
Universita Cattolica del Sacro Cuore Sede di Roma

Research

Keywords: PDIA3, STAT3, IL6, microglia, glioma, punicalagin

Posted Date: August 4th, 2020

DOI: https://doi.org/10.21203/rs.3.rs-51985/v1

Abstract

Background: Glioblastoma (GB - grade IV glioma) is the most aggressive and common cancer of central nervous system with an overall survival of 14-16 months. The GB tumor microenvironment includes cells of the innate immune system identified as glioma-associated microglia/macrophages (GAMs). It is known that between GAMs and GB cells there is a double interaction, but the role of GAMs is still poorly characterized. The endoplasmic reticulum (ER) protein ERp57, also known as PDIA3, is a thiol oxidoreductase with main function related on glycoprotein folding in endoplasmic reticulum. However, PDIA3 shows different functions. In fact, the various subcellular localizations and binding partners of PDIA3 affect numerous physiological processes and diseases: different regulation and modulation of PDIA3 has been reported in multiple pathologies including neurodegenerative diseases and cancer.

Methods: In the present work, we evaluated in both GB cells and microglia-macrophage cells the expression of PDIA3 using specimens collected after surgical from 18 GB patients. In addition, we studied in vitro microglia-glioma interaction to determine the role of PDIA3 in viability and the activation of both GB and microglia cells. The study was carried using PDIA3-silenced T98G cells and/or using a pharmacological inhibitor of PDIA3 activity (Punicalagin-PUN).

Results: We initially investigated the role of the PDIA3 in GB survival by inquiring The Cancer Genome Atlas dataset. The results indicated that 352 out of 690 patients reported over-expression of PDIA3, which significantly correlated with a ~55% reduction of overall survival. Subsequently, for the first time, we investigated the PDIA3 expression in the tumor and the nearby parenchyma of 18 GB patients and our data showed a significant upregulation (15% vs 10%) of ERp57/PDIA3 in GAMs of tumor specimens respect the microglia present in parenchyma. In addition, we show that conditioned medium (CMs) obtained from both wild type T98G and PDIA3 silenced T98G induced an activation of microglia cells, but the PDIA3 silenced-T98G CMs significant limited the microglia pro-tumor activation probably through a IL-6-STAT3-PDIA3 dependent mechanism.

Conclusion: Our data support the relevant role of PDIA3 expression in GB pathology and link the different activation of microglia to a mechanism a IL-6-STAT3-PDIA3 dependent.

Background

Glioblastoma (GB - grade IV glioma) is the most aggressive and common cancer of central nervous system in adults with over 10,000 new cases in United States per year [**1**]. The first-line treatment consists in a multimodal approach with surgical resection, when possible, followed by radiation therapy and concomitant and adjuvant chemotherapy with Temozolomide [**2**]. However due to its invasiveness and infiltrative behavior, the GB is characterized by an overall survival of 14-16 months. Therefore, this tumour has still an important need to be studied and it is necessary to investigate GB etiopathology to find efficacy therapy. For this purpose, today, both the tumor and the tumor microenvironment are studied.

The GB tumor microenvironment includes cells of the innate immune system identified as glioma-associated microglia/macrophages (GAMs) that represent the largest population infiltrating GB tumor [3]. GAMs possess different dynamic states of activation: the M1 state, which is tumor suppressive, and the M2 state, which is tumor supportive, contributing to tumor growth. These different 2 phenotypes are thought to reflect a spectrum of plastic functional conditions rather than a set of discrete activation states [4; 5]. However, although it is known that between GAMs and GB cells there is a double interaction where the first support the latter and *viceversa*, the role of GAMs in the GB context is still poorly characterized.

The endoplasmic reticulum (ER) protein ERp57, also known as PDIA3, GRP58, ERp60 is a thiol oxidoreductase and is a member of the protein disulfi de isomerases (PDIs) family that counts members with different localization and functionality. PDIs protein family have a TRX-like domain and its active or inactive form restrict the PDIs mostly to the endoplasmic reticulum [6; 7], however different localizations have been reported [8]. The first and main function of PDIA3 is related on glycoprotein folding in endoplasmic reticulum (ER) [9]. In fact, PDIA3 interacts with calnexin and calreticulin regulating the folding of newly glycoproteins catalysing the formation and disruption of disulfide bonds between cysteine residues [10; 11]. However, PDIA3 plays different functions (depending on cellular localization) beyond its abilities in the ER. In the cell membrane, for example, PDIA3 acts as a membrane receptor for 1α, 25-dihydroxy-vitamin D3 [12; 13]. In the cytoplasm, PDIA3 co-localizes with NF-κB or mTOR, forming in the latter case a complex that has been implicated in various developmental processes [14]. In the nucleus, PDIA3 directly interacts with DNA or enhances the DNA-binding of the signal transducer and activator of transcription 3 (STAT3) complex, influencing binding of the transcription factor to DNA, and facilitating nuclear import and export of transcription factor [15; 16; 17]. Therefore, the various subcellular localizations and binding partners of PDIA3 affect numerous physiological processes and diseases. In fact, different regulation and modulation of PDIA3 has been reported in multiple pathologies including neurodegenerative diseases [18; 19], and cancer [20; 21; 22]. Moreover, PDIA3 expression level has been evaluated as a biomarker in several conditions [23; 24] and could be a novel pharmacological target. PDIA3 signalling has a pharmacological natural inhibitor, Punicalagin (PUN). Punicalagin is a natural compound deriving from the secondary metabolism of different plants and represents the known largest molecular weight polyphenol found in forms alpha and beta in pomegranates (Punica granatum), in Terminalia catappa and Terminalia myriocarpa and in Combretum molle. PUN shows several properties among which anti-inflammatory activity and recent studies shown the binding with PDIA3 and its redox activity inhibition [25].

In the last years, our group has investigated the role of GAMs in different murine and human models of GB microenvironment, looking at GAM polarization status [26], at the involvement of mTOR pathway in GAM activation [27; 28], as well as at the role of chemokine receptor CCR5 in GAM migration and activation [29]. In addition, recently, we have also investigated VEGFR-1 expression in GAMs [30]. In the present work, we evaluated both in GB cells and microglia-macrophage cells the expression of PDIA3 in GB specimens collected after surgical from 18 patients. In addition, we studied *in vitro* microglia-glioma interaction to determine the role of PDIA3 in viability and the activation of both GB and microglia cells.

The study was carried using PDIA3-silenced T98G cells and a pharmacological block using PUN. For the first time in the context of glioblastoma, we show a biochemical involvement of PDIA3 in the activation of both GB cells and GAMs.

Methods And Materials

Materials

Cell culture reagents [Dulbecco's modified Eagle's medium (DMEM) and Fetal calf serum (FCS)] were from Invitrogen Corporation (Paisley, Scotland). Antibiotics were from Biochrom AG (Berlin, Germany). Puromycin was from VWR Life Science and Punicalagin was from Sigma Aldrich. The human recombinant interleukin 1β (IL1β), human IFN γ and recombinant human Tumor necrosis factorα (TNFα) were purchased from R&D System. β -actin (clone AC-74) mouse monoclonal antibody was from Sigma Aldrich; rabbit monoclonal phospho-STAT3 (Tyr705) and mouse monoclonal STAT3 (124H6) was from Cell Signaling, goat polyclonal AIF-1/IBA1 was from Novus, anti-ERp57/PDIA3 was kindly provided by Prof. Fabio Altieri, rabbit polyclonal IκBα was from Santa Cruz Biotechnology, Inc; rabbit polyclonal 4EBP1 (Cat. No.: A300-501A) was purchased from Bethyl Laboratories, Inc (Montgomery, TX, USA), anti-rabbit was purchased from Jackson ImmunoResearch Laboratories, Inc. (Cat. No.: 111-035-045, West Grove, PA, USA), and anti-mouse was purchased from Sigma-Aldrich (Cat. No.: A3682—St.Louis, MO, USA).

Patients and Specimens

We studied 18 adults of the 42 patients already described [**26**] who underwent surgery for primary GBM at the Neurosurgery Department, Fondazione Policlinico Gemelli" (Rome, Italy), from March 2005 to September 2011. Diagnosis of GB was established on histological examination according to the WHO classification (grade IV) of tumors of the CNS. In all cases a total tumour removal was achieved, allowing us to obtain tissues samples from both the tumour and the surrounding macroscopic normal brain tissue (between 1 cm and 2 cm from the tumour border; larger resections were performed in tumours that grew far from eloquent areas). The demographic characteristics of patients are reported in Table 1. All patients provided written consent to use their specimens for research and the research proposal was approved by the local ethics Ethical Committee [**26**].

Table 1
Demographic characteristic of GB patients.

Study cohort (18 patients)	Demographic characteristic	# of patients	% of patients
Age	over 70	5	27.8
	60-70	5	27.8
	50-60	3	16.7
	40-50	3	16.7
	under 40	1	5.6
	NA	1	5.6
Gender	Male	13	72.2
	Female	5	27.8
WHO grade classes	IV	18	100
Tumor	Primary	14	77.8
	Recurrent	4	22.2
Tumor location	Frontal	6	33.3
	Occipital	2	11.1
	Temporal	5	27.8
	Parietal	1	5.6
	Tempo-Parietal	1	5.6
	NA	3	16.6

[a]NA: not available

Tissue preparation

Human tumor tissue obtained from surgical resection of patients with grade IV GBM were fixed in 4% paraformaldehyde in 0.1 M phosphate buffer pH 7.6 overnight at 4°C. Dehydration of tissue was through a series of 80%, 95% ethanol one hour each followed by 100% ethanol overnight. Two 100% xylene washes were done for 1 hour each and then 1 hour in 60°C Paraplast Plus (Tyco/Healthcare, Mansfield,

MA). After a change of Paraplast Plus, tissue was incubated in a 60°C vacuum oven for 2 hours prior to placing in molds to cool and solidify. Sections, 3 µm thick, were cut and collected on the superfrost plus slides (Fisher).

Immunohistochemistry

Double-staining

The PT Link (Dako) was used to deparaffinize and rehydrate the sections and unmask antigen sites. Slides were immersed in 10 mM citrate buffer, pH 6.0, for 10 min at 97°C and then cooled and washed in TBS. Endogenous peroxidase activity was inhibited by incubating the slides with Peroxide Block (ScyTek Laboratories, Utah, USA) for 7 minutes. After washing in distilled water and then in TBS, sections were treated with Avidin-Biotin Kit (Biocare-Medical) to reduce background staining caused by endogenous biotin. After 3 washes in TBS, nonspecific binding was blocked by 10 minutes incubation with Background Punisher (Biocare-Medical). Sections were incubated over-night at 4°C with Goat Anti-Human Iba1 polyclonal antibody (Novus Biologicals) 1:250, washed extensively in TBS and subsequently incubated with Ultratek HRP kit (ScyTek Laboratories) and the reaction was revealed by incubation with 3,3'-diaminobenzidine (Biocare-Medical). The same slides were washed extensively in distilled water and TBS and blocked with Background Punisher (Biocare-Medical). The rabbit anti-PDIA3 antibody 1:500 was incubated over-night at 4°C and after 3 washes in TBS, slides were incubated with the MACH 2 Rabbit HRP-Polymer (Biocare-Medical). The PDIA3-associated signal was then revealed by incubation with Vina Green chromogen kit (Biocare-Medical).

Immunostaining Analysis

For quantitative analysis, two blinded examiners counted the number of PDIA3+, IBA1+, or both PDIA3+ and IBA1+ cells in a number of 50 cells total in three randomly different areas of the slides. In particular, two blinded examiners have examined three different areas of the same slides and have counted 50 cells that included the number of positive cells for each antibody, the number of positive cells for both antibodies and the number of negative cells [31]. In total, the average of six counts was reported as percentage.

Cell cultures

The human microglia cell line (CHME-5; RRID: CVCL_5J53) was kindly provided by professor Pierre Talbot [32]. CHME5 cells were grown in DMEM media containing 10% FCS and antibiotics; experimental conditions were reached with DMEM at low concentration of FCS (1%) and cells were splitted at the 80% of the confluence.

Glioblastoma cell line T98G [T98-G] (ATCC® CRL-1690™) was kindly provided by professor Grazia Graziani (Tor Vergata University- Rome). T98G cells were grown in DMEM containing 10% FCS and antibiotics. Experimental conditions were reached with DMEM containing 1% FCS and antibiotics. Cells were splitted at the 80% of the confluence. All the experiments received institutional approval. Conditioned media from activated glioma cells was generated following a protocol described before [**28**]. Briefly, Basal Conditioned Media (B-CM) was prepared with 4 hours incubation in plain medium, followed by 3 washes with phosphate buffered saline (PBS) and addition of fresh plain medium for 24 hours. After that, CM was collected, centrifuged to remove cellular debris and stored at -80°C. Prestimulated Conditioned Media (PS-CM) was prepared with 4 hours incubation with a mixture of cytokines (10 ng/ml TNFα, 10 ng/ml IL1β, 10 UI/ml hIFNγ called TII), followed by 3 washes with PBS and addition of fresh plain medium for 24 hours. After that, the CM was collected, centrifuged and stored at -80°C.

RNA interference (siRNA)

siRNA for PDIA3 was kindly provided by professor Fabio Altieri (University of Rome – La Sapienza) and Lipofectamine™ 2000 was purchased from Invitrogen. The day before transfection, 5×10^5 cells per well were seeded in a 6-well plate and were grown in normal conditions. The transfection was carried out according to the manufacturer's instructions and the siRNA was used at 1 μg per milliliter final concentration. Cell lines were incubated 6 hours with the transfection complex under their normal conditions and after 48 hours incubation the selection with puromycin at 1μg/ml was conducted. Cells were grown with puromycin for at least two weeks and then PDIA3 gene and protein expression were carried out.

Nitrite assay

iNOS activity was assessed indirectly by measuring nitrite accumulation in the incubation media. Briefly, an aliquot of the cell culture media (80 μL) was mixed with 40 μL Griess Reagent (Sigma-Aldrich, St Louis, MO, USA) and the absorbance measured at 550 nm in a spectrophotometric microplate reader (PerkinElmer Inc. Waltham, MA, USA). A standard curve was generated during each assay in the range of concentrations 0–100 μM using $NaNO_2$ (Sigma-Aldrich) as standard. In this range, standard detection resulted linear and the minimum detectable concentration of $NaNO_2$ was ‡ 3.12 μM. In the absence of stimuli, basal levels of nitrites were below the detection limit of the assay at all the time points studied. The levels of NO were normalized with the protein content determined by Bradford's method (Bio-Rad, Hercules, CA, USA) using BSA as standard.

Urea assay

Urea levels in CHME5 and T98G cells were detected by the QuantiChrom Urea Assay kit (BIOassay System, Hayward, CA, USA), used according to the manufacturer's instructions. Briefly after 48h of

incubation with the B-CM and PS-CM, an aliquot of cell culture media (50 µl) was mixed with 200 µL Urea Reagent (Bioassay system) and the absorbance measured at 430 nm in a spectrophotometric microplate reader (PerkinElmer Inc., MA, USA). A standard curve was generated during each assay in the range of concentrations 0-100 µg/ml using Urea as standard. In this range, standard detection resulted linear and the minimum detectable concentration of Urea was 3.12 µg/ml. The protein content in each sample was determined by Bradford's method (Biorad, Hercules, CA, USA) using bovine serum albumin as standard.

Cytometer analysis

For intracellular analysis, cells were fixed and permeabilized with Fix/Perm buffer (ThermoFisher Scientific, MA, USA) and then incubated with primary monoclonal antibody anti-ARG1 (C-2) (Santa Cruz Biotechnology, Inc, TX, USA). Secondary monoclonal Antibody Goat anti-Mouse Alexa Fluor®-488 (ThermoFisher Scientific, MA, USA) was used. The purity of cell preparations was assessed by cytofluorimetric staining. Unstained cells were used as a negative control.

Cell Viability and Toxicity

In order to discriminate viable, non-viable cells and apoptosis detection in flow cytometry, cells were incubated with Propidium Iodide and Annexin V-FITC (Novus Biological - NBP2-29373). The assay was conducted following the manufacturer's instructions. Compensation control cells were provided and unstained cells were used as negative control. Flow cytometry analysis was conducted with FC 500 (Beckman Coulter, Brea, CA) and the data were analyzed with Kaluza software (Beckman Coulter, Brea, CA). At least 50,000 events were acquired.

The cell viability was also measured using a specific luminescence kit: CellTiter-Glo® Luminescent Cell Viability Assay (Promega, WI, USA). Cell mortality was detected using a specific fluorescence kit: RealTime-Glo™ MT Cell Viability Assay (Promega, WI, USA). The assays were carried out according to the manufacturer's instructions.

ROS assay

Detection of intracellular reactive oxygen species (ROS) were reached using H2DCF-DA [2,7-dichlorodihydrofluorescein diacetate (10mM)] as probe. Briefly, cells were treated for 48h and after that, the incubation medium was replaced by Balanced Salt Solution (BSS - NaCl 124 mM, KCl 5.8 mM, dextrose 10 mM, Hepes 20 mM, CaCl2(H2O)2 0.3 mM) and cells were incubated for 30 minutes at 37°C. At the end of the incubation time H2DCF-DA 20 µM were added and cells were incubated for 45 minutes at 37°C.The fluorescence signal was quantified using a microplate fluorescence reader (VictorXTM4 microplate reader, PerkinElmer Inc, Waltham, Ma, USA), using 485 nm as excitation and 535 nm as emission wavelength.

mRNA analysis in real time PCR

Total cytoplasmic RNA from cell lines was extracted using the TRIzol reagent protocol and RNA from FFPE tissues was extracted using the Absolutely RNA FFPE Kit (Agilent, CA, USA) using the manufacturer's instructions. RNA concentration was measured using the Qubit™ RNA HS Assay Kit (Thermo Fisher Scientific). Aliquots (1 µg) of RNA were converted to cDNA using random hexamer primers. Quantitative changes in mRNA levels were estimated by real time PCR using the following cycling conditions: 35 cycles of denaturation at 95 °C for 20 s; annealing and extension at 60 °C for 20 s; using the Brilliant III Ultra-Fast SYBR® Green QPCR Master Mix (Stratagene, CA, USA). PCR reactions were carried out in a 20-µL reaction volume in AriaMX real time PCR machine (Agilent, CA, USA). Genes' expression was evaluated using the following primers: Human PDIA3 Forward: GCCACAGTCTTGTCCTCAAACTTG and reverse: TTCCTAAAAGCAGCCAGCAACTTG; human COX2 forward: TTGCTGGCAGGGTTGCTGGTGGTA and reverse CATCTGCCTGCTCTGGTCAATCGAA3; human IL 6 Forward: GGCTCATTCTGCCCTCGAGCC and Reverse: GGACCGAAGGCGCTTGTGGAG; human IL-1β Forward: AGCCATGGCAGAAGTACCGT and Reverse: TCCATGGCCACAACAACTGA; human GAPDH Forward: CCCTCGCCATGGTAAATACAT and Reverse: ACTGGATGGTACGCTTGGTCT. Relative mRNA concentrations were calculated from the take-off point of reactions (threshold cycle, Ct) using the comparative quantitation method provided by AriaMX software and based upon the -ΔΔCt method. Ct values for GAPDH expression served as a normalizing signal.

IL6 quantification and multiple cytokines analysis

IL6 levels in the incubation medium were detected using a specific enzyme-linked immunosorbent assay (ELISA - R&D System, MN, USA). The assay was carried out according to the manufacturer's instructions.

Levels of cytokines and chemokines from culture media were detected using the Proteome Profiler Human Cytokines XL kit (R&D System, MN, USA). The assay was conducted following the manufacturer's instructions. 500µL of cell culture supernatant was run on each assay. Each spot was measured with image analysis software and the average pixel density of negative control spots was taken as background and subtracted. Then, each dataset was represented with GraphPad Software Prism and student t-test between B-CM and B-CM sh and PS-CM and PS-CM sh was conducted.

Western immunoblot

The cells were lysed in RIPA buffer (1 mM EDTA, 150 mM NaCl, 1% igepal, 0.1% sodium dodecyl sulfate, SDS, 0.5% sodium deoxycholate, 50 mM Tris–HCl, pH 8.0) (Sigma-Aldrich, MO, USA) containing protease inhibitor cocktail diluted 1:250 (Sigma–Aldrich, MO, USA). The protein content in each sample was determined by Bradford's method (Biorad, CA, USA) using BSA as standard. A 100 µg aliquot of protein was mixed with 4X Bolt™ LDS Sample Buffer (Cat. No.: B0008 – Invitrogen, CA, USA) and 10x Bolt™ Sample Reducing Agent (Cat. No.: B0009 - Invitrogen, CA, USA), boiled for 5 min, and separated through 4-

12% bis-tris plus gel (Invitrogen, CA, USA). Apparent molecular weights were estimated by comparison to colored molecular weight markers (Sigma-Aldrich, MO, USA). After electrophoresis, proteins were transferred to nitrocellulose membranes by iBlot™ 2 Gel Transfer Device (Invitrogen, CA, USA). The membranes were incubated in the presence of the primary and secondary antibody in the iBind™ Flex Western Device (Cat. No.: SLF2000 - Invitrogen™, CA, USA) for βactin and PDIA3. Primary antibody for IκBα, phospho-STAT3 and total STAT3 were incubated overnight with gentle shaking at 4°C. Each primary antibody diluition was 1:1000. Primary antibody was removed, membranes washed 3 times in Flex Solution, and further incubated for 1h at room temperature in the presence of specific secondary antibody diluted 1:15000 for anti-rabbit and 1:3000 for anti-mouse. Following three washes in Flex Solution, bands were visualized by incubation in ECL reagents (Thermo Scientific™) and exposure to Hyperfilm ECL (GE Healthcare NY, USA).

Statistical analyses

Data were described as median ± Standard Deviation (SD) or SEM as indicated in figure legends. Statistical analysis of the differences between pairs of groups was performed by Student's t test. For multiple comparisons ANOVA analysis, followed by Sidak's post-test, was used. Statistical significance was determined at $\alpha = 0.05$ level. Differences were considered statistically significant when $p < 0.05$. Statistical analysis was performed with GraphPad software Prism version 7.04 (GraphPad Software, San Diego, CA, USA).

Results

PDIA3 in Glioblastoma specimens

Relevance of PDIA3 expression in GB patients' survival

We initially investigated the role of the PDIA3 in GB survival by inquiring the TCGA (The Cancer Genome Atlas) database [https://xenabrowser.net/]. The results indicated that 352 out of 690 patients (dataset: TCGA lower grade glioma and glioblastoma) reported over-expression of PDIA3, which significantly correlated with a ~55% reduction of overall survival (**Figure 1**). These data support the relevant role of PDIA3 expression in GB aggressiveness.

Difference in PDIA3 expression between tumour and brain parenchyma in human GB specimens

In order to analyze the distribution of PDIA3 expression in GB, we examined the tumour and surrounding parenchyma of the same patients in tissue specimens collected after surgical removal of the tumour from 18 patients diagnosed with GB. Unexpectedly, the tumour tissue presented a significantly lower

number of PDIA3 stained cells in comparison with the surrounding parenchyma (**Figure 2A and B**). In fact, in the parenchyma about 50% of the cells were positive for PDIA3, while in the tumour the percentage of cells expressing PDIA3 was about 40% (**Figure 2C**). Interestingly, the staining of PDIA3 is not the same for all types of cells: there are cells that presented nuclear membrane strengthening and cells in which the cytoplasm resulted also positive for PDIA3. These data suggest that PDIA3 is expressed by GB cells as well as by cells of the tumour-associated microenvironment. Therefore, since microglia represent the cell type that mostly infiltrates the tumor we analyzed the expression of PDIA3 in GAMs. By double staining for PDIA3 and Iba1 (a macrophage-microglia marker) in these samples, we found that the percentage of microglia-macrophages expressing PDIA3 present in the tumour was significantly higher than in the parenchyma (**Figure 2D**). In fact, taking into account only the microglia-macrophage cell population, in the tumour 15% of the Iba1 positive cells also expressed PDIA3, whereas in the parenchyma the percentage of double positive cells was 10%. The number of cells positive for Iba1 in the 18 patients studied was similar between the parenchyma and the tumour.

Effects of PDIA3 on T98G glioblastoma cell line activation and vitality

In order to study the effects of PDIA3 on the release of chemokines and cytokines and on viability of glioma cells, the PDIA3 gene was silenced in T98G cells or a pharmacological inhibitor of PDIA3 activity (punicalagin-PUN) was used. In particular after PDIA3 gene silencing on T98G cell line (about 35% of PDIA3 in both mRNA and protein level was silenced- **Figure S1**) the T98G showed a reduction of 40% in IL6 and COX2 gene expression and an increment of more than 50% in IL1β expression comparing to basal conditions of wild type T98G (**Figure 3**). In addition, we evaluated a panel of 105 cytokines and chemokines released from both PDIA3 silenced-T98G and wild type T98G under basal condition (the media collected was called B-CM). When PDIA3 is silenced a significant increase of Fibroblast Growth Factor (FGF-19), Platelet-derived growth factor (PDFG-AA) and Osteopontin occurred, while a significant decrease of insulin-like growth factor-binding protein 2 (IGFBP2) and IL8 is proved (**Figure 4C**). In addition, PDIA3-silenced T98G released cytokines and chemokines never produced from the wild type T98G such as Angiopoietin 2, Complement factor D, DKK-1, MCSF, resitin and uPAR (**Figure 4D**).

Moreover, in order to study the inflammatory activation of glioma cells we studied also the effects of PDIA3 on TII-stimulated both wild type and PDIA3-silenced T98G. Therefore, when wild typeT98G were treated with TII for 8 hours, data shown an increment of IL6, COX2 and IL1β compared to calibrator of more than 600-fold, 115-fold and 800-fold respectively. When PDIA3 was silenced and under the same experimental conditions, PDIA3-silenced T98G showed still an increase in the same gene expression, but the PDIA3 silencing limited the increment of about 50% for COX2 (115-fold vs 57-fold) and about 25% for IL1β (800-fold vs 590-fold) (**Figure 5**). In addition, after 4 hours of TII stimulation, 3 washes and 24 hours of incubation with fresh media, we collected the media (called PS-CM) and we evaluated the same panel of 105 cytokines and chemokines released from both PDIA3 silenced- and wild type T98G. In PDIA3-silenced PS-CM Chitinase 3-like, GM-CSF, Monocyte Chemoattractant protein 2 (MCP3 or CCL7) and C-C

Motif Chemokine Ligand 20 (CCL20 or Macrophage Inflammatory Protein 3 - MIP3A) are increased and Cystatin C, Emmprin, IGFBP2, Monocyte Chemoattractant protein 1 (MCP1 or CCL2), C-X-C motif chemokine 11 (CXCL11), Osteopontin and Thrombospondin-1 are decreased (**Figure 6C**). In addition, PDIA3-silenced T98G released cytokines and chemokines never produced from the non-silenced counterpart such as Complement factor D, Granulocyte colony-stimulating factor (G-CSF) and Chemokine (C-C motif) ligand 3 and 4 (CCL3/CCL4) (**Figure 6D**).

In flow cytometry analysis with Annexin V-Propidium Iodide assay, the effect of the block of PDIA3 activity induced by PUN on viability of wild type T98G cell was tested. We tested two different concentrations of PUN, 5μM and 50μM. After 24 hours of treatment, viable T98G cells were more than 70% in 5μM PUN with 15% of cells in early apoptosis (**Figure 7**). Punicalagin 50μM showed high toxicity with 80% of non viable cells, but through a necrotic way.

Effects of PDIA3 gene silencing in microglia-glioma interactions.

Effects of CMs from both PDIA3-silenced and wild type T98G on CHME-5 viability and activation.

Based on previous data showing the toxicity of CMs from glioma cells, CHME-5 were exposed to a challenge of B-CM and PS-CM from both wild-type and PDIA3-silenced T98G. The viability and the status of microglia activation were evaluated. Under a phase contrast electronic microscope, CHME-5 treated 24 hours with B-CM and PS-CM from PDIA3-silenced T98G preserve the same morphology as when CHME-5 were treated with CMs obtained by wild type T98G. Conversely, when microglia cells are treated with PDIA3-silenced CMs the number of cells is increased compared to treatments with CMs from wild type T98G (**Figure 8**). In particular, the number of CHME-5 cells was between 30-40% more (the same as control) when treated with PDIA3 silenced T98G respect when treated with wild type T98G CMs. However, when we analyze the 24h-viability of CHME-5 measuring a direct inhibition of PDIA3 elicited by 5μM PUN, we found a significant reduction of CHME-5 viable cells when treated with PUN respect to un-treated cells. In particular, we found more than 70% of viable cells and 20% in early apoptosis stage (**Figure 9**).

These data indicate that the PDIA3 pathway is important for microglial cell survival (tested using PUN on CHME-5) but that the absence of the same pathway on glioma cells does not affect microglial viability as well (tested using CMs obtained from PDIA3–silenced T98G on CHME-5).

As parameter of M2 (or anti-tumor) activation, we measured urea release in the medium and the activity of ARG1 of CHME-5 in flow cytometry. Urea release, after 48 hours was reduced of 40% in CHME-5 treated with PDIA3-silenced T98G B-CM compared to wild type T98G B-CM. Similarly, CHME-5 treated with PS-CM obtained from PDIA3-silenced T98G shown 40% of urea decrease compared to cells treated PS-CM of T98G (**Figure 10A**). To confirm the reduction of the M2 phenotype we investigated the ARG1 expression

of CHME-5 on flow cytometry when cells are treated with CMs. In particular, measures of fluorescence intensity from CHME-5 treated with B-CM and PS-CM from wild type T98G and B-CM and PS-CM from PDIA3-silenced T98G were collected after 24 hours of stimulation; accordingly with urea data, the expression of ARG1 when CHME-5 were treated with B-CM from wild type T98G was increased compared to B-CM from PDIA3-silenced T98G (**Figure 10B**). Similarly, PS-CM treatments shown enhanced expression of ARG1 when compared to PS-CM from PDIA3-silenced T98G (**Figure 10C**).

As parameter of M1 (pro-tumor) activation, we measured IL6 release from CHME-5 treated with CMs. No change was reported expect that IL6 release was reduced by half after 24 hours when cells were treated with PDIA3-silenced T98G PS-CM compared when the cells were treated with PS-CM obtained from wild-type T98G (**Figure 11A**). Moreover, we investigated a transcription factor sensitive to cytokine levels: signal transducer and activator of transcription 3 (STAT3). In 2 hours western blot analysis, CHME-5 treated with CMs from wild type T98G and PDIA3-silenced T98G shown increasing levels of phospho-STAT3 in treatment with PS-CM from PDIA3-silenced T98G compared to PS-CM from wild type T98G (**Figure 11B**). On the contrary, total STAT3 is increased in the B-CM from PDIA3-silenced T98G compared to B-CM from T98G while it is reduced in the PS-CM from PDIA3-silenced T98G compared to PS-CM from T98G (**Figure 11B**). Similar changes in STAT3 are also reported after 24 hours of treatment (**Figure S2**).

Therefore, all these data suggest that a partial block of PDIA3 on T98G could be beneficial on microglia activation tend to reduce the M2 phenotype without exacerbate a pro-inflammatory activation.

Effects of PUN on microglia pro-inflammatory activation

In parallel, we also tested the effects of a pharmacological inhibition of PDIA3 on CHME-5 pro-inflammatory activation. Therefore, CHME-5 cells were treated for 24 or 48 hours with TII alone or in combination to serial dilutions of PUN [1nM-100μM]. Nitrites levels were significantly reduced when TII is combined with 5μM PUN going from 18 μM/mg proteins (TII alone) to 1.2 μM/mg proteins (TII + 5μM PUN) on average (**Figure 12A**). The NO data of dose range were reported in **Figure S3**. In addition to NO levels, an evaluation of the intracellular production of total reactive oxygen species, was carried out measuring the species with the fluorescent dye, 2',7'-dichlorodihydrofluorescein diacetate (H2DCF-DA) and treating CHME-5 for 48 hours with TII alone and in association with 5μM PUN. Data shown a significant reduction of fluorescence in TII combined with PUN and the compound given alone (**Figure 12B**) reinforcing the idea of multi-level anti-inflammatory activity. In addition, IL6 release in the culture media of CHME-5 was evaluated after 24 hours of treatment with 5μM PUN and data were compared to IL6 release under basal conditions. Accordingly with the reduction of IL 6 release on PDIA3-silenced T98G, on CHME-5 treated with PDIA-silenced CMs, IL6 release is also reduced when cells are treated with 5μM PUN (78.5 pg/ml on average) compared to control (125 pg/ml on average) (**Figure 12C**). These data clearly indicated a strong correlation between IL6 and PDIA3.

To explain the anti-inflammatory effects of PUN on CHME-5 we tested the involvement of the NFκB pathway and in particular, we measured IκBα levels (a NFκB inhibitor). Briefly, 2 hours experiments were

carried out and we reported an increment of IκBα in the treatment with PUN with an increment of 93-fold were given alone and of 43,5-fold and 41,8-fold in TII combined with PUN and B-CM combined with PUN respectively (**Figure 13**). Taken together, data confirm an involvement of PDIA3 on microglia activation and suggests multi-level anti-inflammatory activity of PUN in microglia cells.

Discussion

For the first time we evaluated the expression of ERp57/PDIA3 in glioma-associated microglia/macrophages of human glioblastoma specimens. In particular, we investigated the ERp57/PDIA3 expression in the tumor and the nearby parenchyma of 18 GB patients and our data shown an upregulation of ERp57/PDIA3 in GAMs of tumor specimens (**Figure 2**) supporting the idea of its potential involvement in cellular and molecular processes of GB as well as different cancers. In fact, ERp57/PDIA3 has been evaluated as therapeutic target in cancer progression for i.e. in renal cancer and in hepatocellular carcinoma [**21; 33**]. In addition, in several cancer cell lines the knockdown of ERp57 affects different pathways involved in its physiological functions [**34; 14**]. In this scenario, using a siRNA we made a knockdown of ERp57/PDIA3 in T98G glioblastoma cell lines (**Figure 1 suppl**) and we investigated the effects on mRNA expression of IL6, IL1β and COX2 genes (**Figure 3**). Interestingly, ERp57/PDIA3 knockdown reduced the basal expression of IL6 and COX2 genes but increased IL1β expression (**Figure 3**), suggesting a pivotal role of PDIA3 on inflammatory activation of T98G. Accordingly, when we challenged for 4 hours with TII both PDIA3- silenced and wild type T98G we obtained a limited increase of IL1β and COX2 when we measured the gene expression on PDIA3-silenced T98G in comparison to wild type T98G, whereas IL6 gene expression was not modified or tend to be up regulated (**Figure 5**). Accordingly, IL6 regulates the inflammatory activation by decreasing pro-inflammatory cytokines and upregulating anti-inflammatory cytokines [**35**]. Due to its dual role in inflammation, IL6 upregulation can be linked to the total reduction of inflammatory parameters when PDIA3 is silenced [**36**]. In addition, COX2 overexpression in cancer has been extensively reported and contributes to tumor development and progression [**37; 38; 39; 40**]. COX2 is also overexpressed in many gliomas and it is correlated with tumor grade and shorter survival [**41; 42**]. PDIA3-silenced T98G showed a downregulation of gene expression of COX2 when treated with activating stimuli reinforcing the idea of beneficial role of ERp57/PDIA3 inhibition in glioma patients.

Using the microglia-glioma interaction paradigm in functional experiments with T98G cells used as human glioma model and CHME-5 cells as human microglia model, we investigated the involvement of ERp57/PDIA3 in the bi-directional interaction between glioma and microglia cells. In this context, we produced conditioned media from both PDIA3-silenced and wild-type T98G cells and evaluated the urea release of CHME-5 when treated with CMs. In our studies, we used the urea release as parameter of M2 activation. Arginase-1 (ARG1) converts arginine to ornithine and urea, competing with nitric oxide synthase (NOS), usually used as M1 marker which utilizes arginine to produce nitric oxide [**43; 44**]. Our previous data shown an increase of urea production when CHME-5 were treated with CMs from wild type T98G, reinforcing the M2 phenotype [**28**]. Here, we interestingly reveal a phenotypic modification of CHME-5 by detaching the cells from the glioma-induced M2 phenotype with changing in urea production

and in morphology. In fact, cytofluorimetric analysis showed less expression of ARG1 (**Figure 10**) without an upregulation of NOS (**data not shown**) and in vitro assays shown a decrease of urea release when CHME-5 were treated with CMs from PDIA3-silenced T98G. Moreover, we investigated the IL6 release in such experimental conditions. In our work, we found that when microglia cells where treated with PDIA3-silenced T98G PS-CM we assist to a decrease in IL6 levels. These data are linked to the decrease of CCL2 and IL6 from GAMs of glioma (mimicked by PDIA3-silenced T98G PS-CM) implicated in glioma growth and invasiveness [**45**]. This, associated with the anti-inflammatory role of IL6 and the urea decrease reported, supports our hypothesis of non-M2 phenotype of microglia. Interleuchin-6 also trigger the JAK/STAT3 pathway and in the GB pathology high levels of IL6 are related to poor outcome and overall survival [**36; 46**]. ERp57/PDIA3 modulates STAT3 signalling [**15**], is present in STAT3-DNA complexes [**16**] and ERp57/PDIA3 up or downregulation is respectively related to cancer progression and inhibition of proliferation through STAT3 [**21; 47**]. IL-10, IL6 and FGF are known STAT3 activators and STAT3 is constitutively activated in gliomas supporting tumorigenesis [**48**]. Moreover, STAT3 suppresses anti-tumor immunity in GB [**49**]. In this scenario, we investigated STAT3 expression when microglia cells interact with wild type T98G glioma cell and PDIA3-silenced T98G. Interestingly, comparing the CMs effects we are faced with opposite effects: on the one hand there is an up regulation of total STAT3 when we treat the cells with PDIA3-silenced B-CM, on the other hand we reported a downregulation when we are looking at the PDIA3-silenced PS-CM. It could be speculated that these opposite ways are led by FGF-19 augmented release in PDIA3-silenced B-CM and IL6 and FGF-19 decreased release in PDIA3-silenced PS-CM. At this stage, it is not possible to directly correlate the effect of PDIA3 silencing to the STAT3 activity but since PDIA3 is related to STAT3 at different levels, taken together these data are reinforcing the idea of a hybrid phenotype neither M1 nor M2 and the hybrid phenotype could be orchestrated by the STAT3 activation pathway. In addition, the different effect on STAT-3 by B-CM and PS-CM may be because to obtain PS-CM, the cells were subjected to stimulation with cytokines that use STAT3 dependent pathways. So the stimulation of these cells can be affected by the inhibition of PDIA3 (being linked to STAT3).

It is known that GAMs interact with glioma cells and the crosstalk is supported by cytokines and chemokines released from both tumor cells and GAMs [**50**]. In particular, glioma cells recruit GAMs through the monocyte chemoattractant protein MCP-1, also known as C-C motif ligand 2 (CCL2) [**51**]. Moreover, the macrophage colony-stimulating factor (M-CSF also known as CSF1), the granulocyte-macrophage colony-stimulating factor (GM-CSF) and the stroma-derived factor (SDF-1 also known as CXCL12) are involved in recruitment and in M2 activation of GAMs [**52; 53; 54**].

In this sense, we evaluated the expression of 105 cytokines and chemokines released from both wild type and PDIA3-silenced T98G cells. Several are the cytokines and chemokines released in B-CM and some of them are pro-angiogenic such as Angiogenin, Angiopoietin 1 and VEGF. Additionally, we reported the release of Macrophage migration inhibitory factor (MIF) but probably such inhibitory effect is mitigated by the release of MCP-1. More generally, T98G glioma cells release chemoattractant factors and activation factors of the innate immune response. In PDIA3-silenced B-CM we reported mostly an enhancement of such responses but on the other hand we shown a significant reduction of IFGBP-2 and

IL8 (**Figure 4**). In concert with releasing factors belonging only to PDIA3-silenced B-CM as Complement factor D and M-CSF, the decrease of IL8 and IGFBP-2, and the increase of FGF-19, Osteopontin, that is involved in enhancing production of IFNγ and reducing production of IL-10, and PDGF-AA, that is a mitogen factor, is linked to the different phenotype experienced in vitro [**45**].

More complex is the situation in PS-CM with 43 cytokines and chemokines released from glioma cells. In fact, PS-CM is a condition that mimics late stage of pathology [**27**] and it's characterized by the release of inflammatory cytokines such as IL6, IL8, C-X-C motif chemokine 10 (CXCL10) also known as Interferon gamma-induced protein 10 (IP-10) as well as GM-CSF and MCP-1 to name a few. Interestingly, when we evaluate the cytokines released by the PDIA3-silenced PS-CM we are in front of a mitigation of the response triggered by activating stimuli with decreased secretion of most of them (**Figure 6**). Some exceptions are chitinase 3-like, secreted by activated macrophages, GM-CSF, which is an activator of microglia, MCP-3, that is a chemotactic and activating factor of cells of inflammatory response, and CCL20, that is chemotactic for lymphocytes. In fact, such chemokines and cytokines are increased and are probably linked to the different number of cells reported in our in vitro assays. Moreover, PDIA3-silenced T98G PS-CM releases also IL-24, G-CSF, LIF and CCL3/CCL4 that are not expressed before in PS-CM. It could be speculated that when PDIA3 is silenced and glioma cells are exposed to an activating stimulus, glioma cells are not able anymore to release high amount of IL6 and IL8 to induce the M2 phenotype in GAMs in concert with the IL-24 release, which is a tumor suppressing protein, and LIF, that inhibits the cell differentiation. Thus, glioma cells continue to attract microglia/macrophages in tumor microenvironment but with other differentiation that could be speculate as tumor resolving. It is clear and interesting that ERp57/PDIA3 knockdown in fact provokes different responses in GAMs and its inhibition could be beneficial and obtained with a natural compound: Punicalagin.

PUN has been demonstrated to affect ERp57/PDIA3 reductase activity as a non-competitive inhibitor [**25**] and neuroinflammation in microglia cells [**55; 56; 57**] but PUN activity in gliomas is poorly characterized and seems to be related to autophagic cell death and apoptosis [**58**]. In this context, we evaluated the anti-inflammatory effect of PUN in microglia cells and we investigated the viability of such cells in flow cytometry and in in vitro assays. It might be hypothesized that PUN effects are correlated to the cell type involved because the anti-inflammatory activity was well established in our experiments but not the pro-apoptotic activity; our dose of 5 micro molar was not enough to trigger a cytotoxic effect while with a ten time higher concentration flow cytometry analysis reveals a toxic effect of PUN.

Conclusion

In conclusion, we confirmed the ERp57/PDIA3 upregulation in glioma specimens with an upregulation in GAMs as well. We also demonstrated a dissimilar activation of GAMs when ERp57/PDIA3 is downregulated in glioma cells with differences both in the products downstream of ARG1 activation and at phenotypic level. We can hypothesize that PDIA3 correlates with STAT3 in glioblastoma cells in a feedback loop with IL6 as protagonist. In fact, IL6 is less secreted if PDIA3 was silenced and IL6 itself had less effect on the glioblastoma cell because IL6-dependent activation passes through STAT3, its

activation may in turn require PDIA3. A block of PDIA3 makes glioblastoma cells less able to condition the surrounding medium in their favor (less M2 parameters released from microglia cells and the survival is inversely linked to the levels of PDIA3 in glioblastoma cells). In glial cells, however, the role of PDIA3 would be more protective. In fact, if PDIA3 is directly inhibited the apoptosis was favorable. Therefore, the ideal would be to inhibit PDIA3 in cancer cells but not in other cells. In this context, glioma cells are still able to retrieve GAMs from the surrounding tissue but with a different activation phenotype. Further studies are necessary to confirm the diverse phenotype caused as well as the use of Punicalagin needs to be confirmed in vivo.

Declarations

Ethics approval and consent to participate

All patients signed an informed consent form, and the experimental protocol was approved by the Ethics Committee of Fondazione Policlinico A. Gemelli (Rome).

Consens for publication

Not Applicable

Availability of data and materials

The datasets used and/or analysed during the current study are available from the corresponding author on reasonable request.

Competing interests

The authors declare that they have no competing interests.

Funding

This study was supported by Fondi Ateneo 2019 to P.N. and Fondi Ateneo 2018 to L.L.

Authors' contributions

MC, GMPC AND FC performed the experiment. MC, GMPC and LL analyzed and interpreted the patient data. LL and FA designed the study. LL and PN interpreted the data. MC draft the manuscript. LL wrote the paper. All authors read and approved the final manuscript

Acknowledgements

Not applicable

List Of Abbreviations

PDIA3: Protein Disulfide Isomerases 3

GB: Glioblastoma

GAMs: Glioma Associated Microglia/macrophages

ER: Endoplasmic Reticulum

ERp57: Endoplasmic Reticulum Protein 57

PUN: Punicalagin

TCGA: The Cancer Genome Atlas

CM: Conditioned Medium

IL6: Interleuchin-6

ERp60: Endoplasmic Reticulum Protein 60

PDI: Protein Disulfide Isomerase

TRX: Thioredoxin Domain

NFκB: Nuclear Factor kappa-light-chain-enhancer of activated B cells

mTOR: Mammalian Target of Rapamycin

STAT3: Signal Transducer and Activator of Transcription 3

CCR5: C-C chemokine Receptor type 5

ROS: Reactive Oxygen Species

TNFα: Tumor Necrosis Factor α

siRNA: small interfering RNA

COX2: Cyclooxygenase-2

IL1β: Interleuchin-1 β

IFNγ: Interferon gamma

B-CM: Basal Conditioned-Medium

PS-CM: Prestimulated Conditioned-Medium

FGF-19: Fibroblast Growth Factor 19

PDGF-AA: Platelet-Derived Growth Factor A-A

IGFBP2: Insulin-like Growth Factor-Binding Protein 2

IL8: Interleuchin-8

DKK-1: Dickkopf-related protein 1

M-CSF: Macrophage Colony-Stimulating Factor

uPAR: Urokinase Receptor

GM-CSF: Granulocyte-Macrophage Colony-Stimulating Factor

MCP-3: Monocyte-Chemotactic Protein 3

CCL20: C-C Chemokine ligand 20

MCP-1: Monocyte-Chemotactic Protein 1

CXCL11: C-X-C motif Chemokine 11

G-CSF: Granulocyte Colony-Stimulating Factor

CCL3/CCL4: C-C Chemokine ligand 3 and 4

ARG1: Arginase-1

NO: Nitric Oxide

IκBα: nuclear factor of kappa light polypeptide gene enhancer in B-cells inhibitor, alpha

NOS: Nitric Oxide Aynthases

CCL2: C-C Chemokine ligand 2

IL-10: Interleuchin-10

SDF-1: Stromal cell-Derived Factor 1

VEGF: Vascular Endotelial Growth Factor

MIF: Macrophage migration Inhibitory Factor

IP-10: Interferon gamma-induced Protein 10

IL24: Interleuchin-24

References

1. Rajaratnam V, Islam MM, Yang M, Slaby R, Ramirez HM, Mirza SP. Glioblastoma: Pathogenesis and Current Status of Chemotherapy and Other Novel Treatments. Cancers (Basel). 2020;12(4):937. Published 2020 Apr 10.
2. Lisi L, Chiavari M, Ciotti GMP, Lacal PM, Navarra P, Graziani G. DNA inhibitors for the treatment of brain tumors. Expert Opin Drug Metab Toxicol. 2020;16(3):195-207.
3. Chen Z, Hambardzumyan D. Immune Microenvironment in Glioblastoma Subtypes. Front Immunol. 2018;9:1004. Published 2018 May 8.
4. Dello Russo C, Lisi L, Tentori L, Navarra P, Graziani G, Combs CK. Exploiting Microglial Functions for the Treatment of Glioblastoma. Curr Cancer Drug Targets. 2017;17(3):267-281.
5. Kvisten M, Mikkelsen VE, Stensjøen AL, Solheim O, Van Der Want J, Torp SH. Microglia and macrophages in human glioblastomas: A morphological and immunohistochemical study. Mol Clin Oncol. 2019;11(1):31-36.
6. Freedman RB, Hirst TR, Tuite MF. Protein disulphide isomerase: building bridges in protein folding. Trends Biochem Sci. 1994;19(8):331-336.
7. Wang L, Wang X, Wang CC. Protein disulfide-isomerase, a folding catalyst and a redox-regulated chaperone. Free Radic Biol Med. 2015;83:305-313.
8. Turano C, Gaucci E, Grillo C, Chichiarelli S. ERp57/GRP58: a protein with multiple functions. Cell Mol Biol Lett. 2011;16(4):539-563.
9. Hettinghouse A, Liu R, Liu CJ. Multifunctional molecule ERp57: From cancer to neurodegenerative diseases. Pharmacol Ther. 2018;181:34-48.
10. Frasconi M, Chichiarelli S, Gaucci E, Mazzei F, Grillo C, Chinazzi A, et al. Interaction of ERp57 with calreticulin: Analysis of complex formation and effects of vancomycin. Biophys Chem. 2012;160(1):46-53.
11. Kozlov G, Gehring K. Calnexin cycle - structural features of the ER chaperone system [published online ahead of print, 2020 Apr 13]. FEBS J. 2020;10.1111/febs.15330.
12. Gaucci E, Raimondo D, Grillo C, Cervoni L, Altieri F, Nittari G, et al. Analysis of the interaction of calcitriol with the disulfide isomerase ERp57. Sci Rep. 2016;6:37957. Published 2016 Nov 29.
13. Khanal R, Nemere I. Membrane receptors for vitamin D metabolites. Crit Rev Eukaryot Gene Expr. 2007;17(1):31-47.

14. Ramírez-Rangel I, Bracho-Valdés I, Vázquez-Macías A, Carretero-Ortega J, Reyes-Cruz G, Vázquez-Prado J. Regulation of mTORC1 complex assembly and signaling by GRp58/ERp57. Mol Cell Biol. 2011;31(8):1657-1671.
15. Chichiarelli S, Gaucci E, Ferraro A, Grillo C, Altieri F, Cocchiola R, et al. Role of ERp57 in the signaling and transcriptional activity of STAT3 in a melanoma cell line. Arch Biochem Biophys. 2010;494(2):178-183.
16. Eufemi M, Coppari S, Altieri F, Grillo C, Ferraro A, Turano C. ERp57 is present in STAT3-DNA complexes. Biochem Biophys Res Commun. 2004;323(4):1306-1312.
17. Guo GG, Patel K, Kumar V, Shah M, Fried VA, Etlinger JD, et al. Association of the chaperone glucose-regulated protein 58 (GRP58/ER-60/ERp57) with Stat3 in cytosol and plasma membrane complexes. J Interferon Cytokine Res. 2002;22(5):555-563.
18. Parakh S, Jagaraj CJ, Vidal M, Ragagnin AMG, Perri ER, Konopka A, et al. ERp57 is protective against mutant SOD1-induced cellular pathology in amyotrophic lateral sclerosis. Hum Mol Genet. 2018;27(8):1311-1331.
19. Gonzalez-Perez P, Woehlbier U, Chian RJ, Sapp P, Rouleau GA, Leblond CS, et al. Identification of rare protein disulfide isomerase gene variants in amyotrophic lateral sclerosis patients. Gene. 2015;566(2):158-165.
20. Padariya M, Kalathiya U, Houston DR, Alfaro JA. Recognition Dynamics of Cancer Mutations on the ERp57-Tapasin Interface. Cancers (Basel). 2020;12(3):737. Published 2020 Mar 20.
21. Liu Y, Wang JX, Nie ZY, Wen Y, Jia XJ, Zhang LN, et al. Upregulation of ERp57 promotes clear cell renal cell carcinoma progression by initiating a STAT3/ILF3 feedback loop. J Exp Clin Cancer Res. 2019;38(1):439. Published 2019 Oct 30.
22. Wise R, Duhachek-Muggy S, Qi Y, Zolkiewski M, Zolkiewska A. Protein disulfide isomerases in the endoplasmic reticulum promote anchorage-independent growth of breast cancer cells. Breast Cancer Res Treat. 2016;157(2):241-252.
23. Xiao B, Wang JG, Han F, Shi YX. Effects of calcium-dependent molecular chaperones and endoplasmic reticulum in the amygdala in rats under single-prolonged stress. Mol Med Rep. 2018;17(1):1099-1104.
24. Choe MH, Min JW, Jeon HB, Cho DH, Oh JS, Lee HG, et al. ERp57 modulates STAT3 activity in radioresistant laryngeal cancer cells and serves as a prognostic marker for laryngeal cancer. Oncotarget. 2015;6(5):2654-2666.
25. Giamogante F, Marrocco I, Cervoni L, Eufemi M, Chichiarelli S, Altieri F. Punicalagin, an active pomegranate component, is a new inhibitor of PDIA3 reductase activity. Biochimie. 2018;147:122-129.
26. Lisi L, Ciotti GM, Braun D, Kalinin S, Currò D, Dello Russo C, et al. Expression of iNOS, CD163 and ARG-1 taken as M1 and M2 markers of microglial polarization in human glioblastoma and the surrounding normal parenchyma. Neurosci Lett. 2017;645:106-112.

27. Lisi L, Laudati E, Navarra P, Dello Russo C. The mTOR kinase inhibitors polarize glioma-activated microglia to express a M1 phenotype. J Neuroinflammation. 2014;11:125. Published 2014 Jul 23.
28. Lisi L, Ciotti GMP, Chiavari M, Pizzoferrato M, Mangiola A, Kalinin S, et al. Phospho-mTOR expression in human glioblastoma microglia-macrophage cells. Neurochem Int. 2019;129:104485.
29. Laudati E, Currò D, Navarra P, Lisi L. Blockade of CCR5 receptor prevents M2 microglia phenotype in a microglia-glioma paradigm. Neurochem Int. 2017;108:100-108.
30. Lisi L, Pia Ciotti GM, Chiavari M, Ruffini F, Lacal PM, Graziani G, et al. Vascular endothelial growth factor receptor 1 in glioblastoma associated microglia/macrophages. Oncol Rep. 2020;43(6):2083-2092.
31. Atzori MG, Tentori L, Ruffini F, Ceci C, Bonanno E, Scimeca M, et al. The anti-vascular endothelial growth factor receptor-1 monoclonal antibody D16F7 inhibits invasiveness of human glioblastoma and glioblastoma stem cells. J Exp Clin Cancer Res. 2017;36(1):106. Published 2017 Aug 10.
32. Janabi N, Peudenier S, Héron B, Ng KH, Tardieu M. Establishment of human microglial cell lines after transfection of primary cultures of embryonic microglial cells with the SV40 large T antigen. Neurosci Lett. 1995;195(2):105-108.
33. Liu M, Du L, He Z, Yan L, Shi Y, Shang J, et al. Increased ERp57 Expression in HBV-Related Hepatocellular Carcinoma: Possible Correlation and Prognosis. Biomed Res Int. 2017;2017:1252647.
34. Gaucci E, Altieri F, Turano C, Chichiarelli S. The protein ERp57 contributes to EGF receptor signaling and internalization in MDA-MB-468 breast cancer cells. J Cell Biochem. 2013;114(11):2461-2470.
35. Scheller J, Chalaris A, Schmidt-Arras D, Rose-John S. The pro- and anti-inflammatory properties of the cytokine interleukin-6. Biochim Biophys Acta. 2011;1813:878–888.
36. Fisher DT, Appenheimer MM, Evans SS. The two faces of IL-6 in the tumor microenvironment. Semin Immunol. 2014;26(1):38-47.
37. Taketo MM. Cyclooxygenase-2 inhibitors in tumorigenesis (part I). J Natl Cancer Inst. 1998;90(20):1529-1536.
38. Taketo MM. Cyclooxygenase-2 inhibitors in tumorigenesis (Part II). J Natl Cancer Inst. 1998;90(21):1609-1620.
39. Trifan OC, Hla T. Cyclooxygenase-2 modulates cellular growth and promotes tumorigenesis. J Cell Mol Med. 2003;7(3):207-222.
40. Hashemi Goradel N, Najafi M, Salehi E, Farhood B, Mortezaee K. Cyclooxygenase-2 in cancer: A review. J Cell Physiol. 2019;234(5):5683-5699.
41. Shono T, Tofilon PJ, Bruner JM, Owolabi O, Lang FF. Cyclooxygenase-2 expression in human gliomas: prognostic significance and molecular correlations. Cancer Res. 2001;61(11):4375-4381.
42. Xu W, Huang Y, Zhang T, Zhao L, Fan J, Li L. Cyclooxygenase-2 gene polymorphisms and susceptibility to hepatocellular carcinoma: A meta-analysis based on 10 case-control studies. J Cancer Res Ther. 2018;14(Supplement):S105-S113.

43. MacMicking J, Xie QW, Nathan C. Nitric oxide and macrophage function. Annu Rev Immunol. 1997;15:323-350.
44. Munder M, Eichmann K, Morán JM, Centeno F, Soler G, Modolell M. Th1/Th2-regulated expression of arginase isoforms in murine macrophages and dendritic cells. J Immunol. 1999;163(7):3771-3777.
45. Arcuri C, Fioretti B, Bianchi R, Mecca C, Tubaro C, Beccari T, et al. Microglia-glioma cross-talk: a two way approach to new strategies against glioma. Front Biosci (Landmark Ed). 2017;22:268-309. Published 2017 Jan 1.
46. West AJ, Tsui V, Stylli SS, Nguyen HPT, Morokoff AP, Kaye AH, et al. The role of interleukin-6-STAT3 signalling in glioblastoma. Oncol Lett. 2018;16(4):4095-4104.
47. Kondo R, Ishino K, Wada R, Takata H, Peng WX, Kudo M, et al. Downregulation of protein disulfide isomerase A3 expression inhibits cell proliferation and induces apoptosis through STAT3 signaling in hepatocellular carcinoma. Int J Oncol. 2019;54(4):1409-1421.
48. Sun X, Wang J, Huang M, Chen T, Chen J, Zhang F, et al. STAT3 promotes tumour progression in glioma by inducing FOXP1 transcription. J Cell Mol Med. 2018;22(11):5629-5638.
49. Chang N, Ahn SH, Kong DS, Lee HW, Nam DH. The role of STAT3 in glioblastoma progression through dual influences on tumor cells and the immune microenvironment. Mol Cell Endocrinol. 2017;451:53-65.
50. Roesch S, Rapp C, Dettling S, Herold-Mende C. When Immune Cells Turn Bad-Tumor-Associated Microglia/Macrophages in Glioma. Int J Mol Sci. 2018;19(2):436. Published 2018 Feb 1.
51. Zhang J, Sarkar S, Cua R, Zhou Y, Hader W, Yong VW. A dialog between glioma and microglia that promotes tumor invasiveness through the CCL2/CCR2/interleukin-6 axis. Carcinogenesis. 2012;33(2):312-319.
52. Pyonteck SM, Akkari L, Schuhmacher AJ, Bowman RL, Sevenich L, Quail DF, et al. CSF-1R inhibition alters macrophage polarization and blocks glioma progression. Nat Med. 2013;19(10):1264-1272.
53. Wang SC, Hong JH, Hsueh C, Chiang CS. Tumor-secreted SDF-1 promotes glioma invasiveness and TAM tropism toward hypoxia in a murine astrocytoma model. Lab Invest. 2012;92(1):151-162.
54. Sielska M, Przanowski P, Wylot B, Gabrusiewicz K, Maleszewska M, Kijewska M, et al. Distinct roles of CSF family cytokines in macrophage infiltration and activation in glioma progression and injury response. J Pathol. 2013;230(3):310-321.
55. Olajide OA, Kumar A, Velagapudi R, Okorji UP, Fiebich BL. Punicalagin inhibits neuroinflammation in LPS-activated rat primary microglia. Mol Nutr Food Res. 2014;58(9):1843-1851.
56. Kim YE, Hwang CJ, Lee HP, Kim CS, Son DJ, Ham YW, et al. Inhibitory effect of punicalagin on lipopolysaccharide-induced neuroinflammation, oxidative stress and memory impairment via inhibition of nuclear factor-kappaB. Neuropharmacology. 2017;117:21-32.
57. Rojanathammanee L, Puig KL, Combs CK. Pomegranate polyphenols and extract inhibit nuclear factor of activated T-cell activity and microglial activation in vitro and in a transgenic mouse model of Alzheimer disease. J Nutr. 2013;143(5):597-605.

58. Wang SG, Huang MH, Li JH, Lai FI, Lee HM, Hsu YN. Punicalagin induces apoptotic and autophagic cell death in human U87MG glioma cells. Acta Pharmacol Sin. 2013;34(11):1411-1419.

Figures

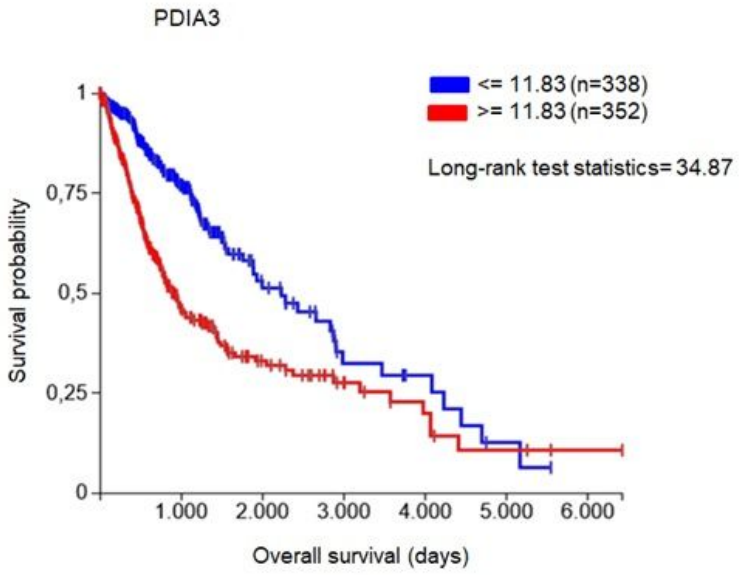

Figure 1

Figure 1

Kaplan Meier gene expression of PDIA3 in a group of glioblastoma patients.

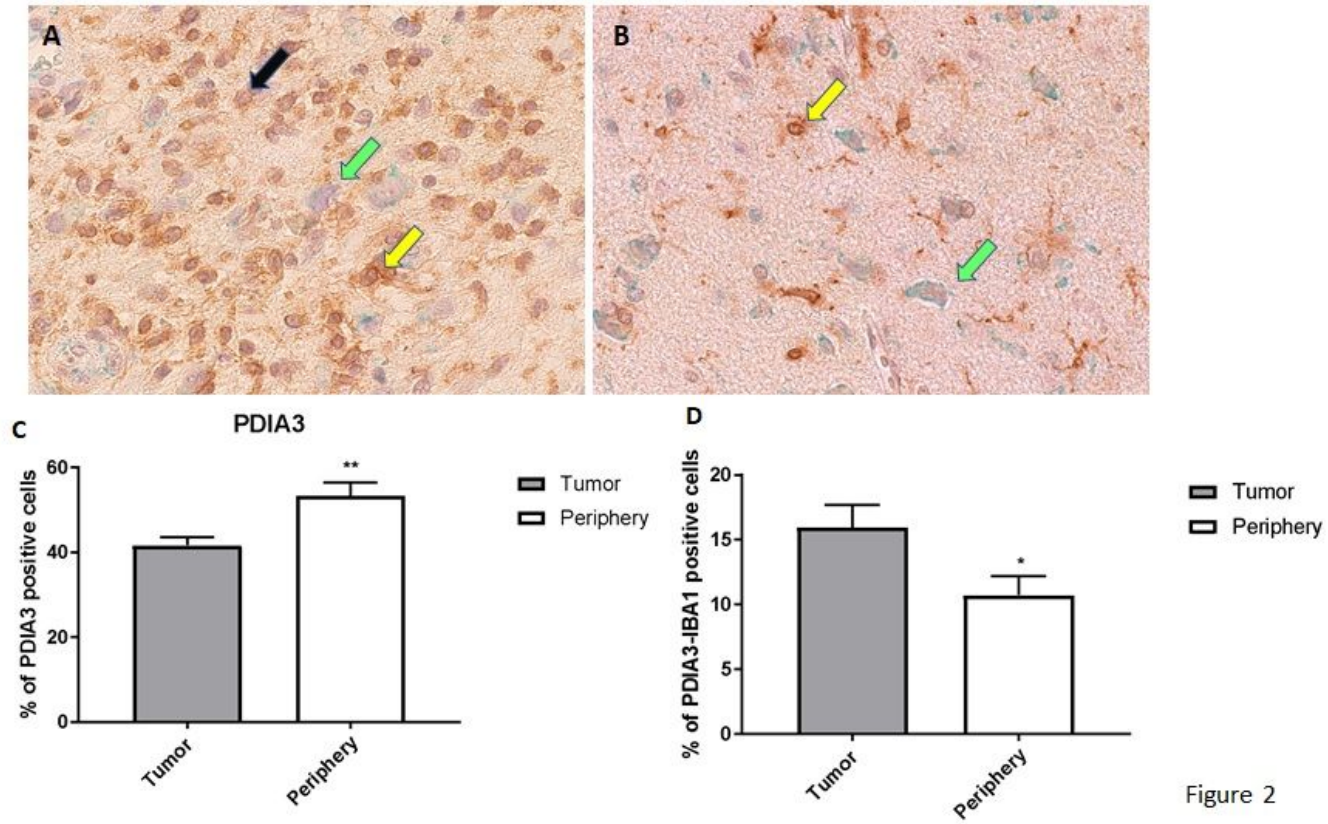

Figure 2

IHC double staining of PDIA3 (green color) and IBA1 (brown color) on glioblastoma specimens. A) Staining of tumor; B) Staining of periphery. Yellow arrow is showing the double staining, black arrow is showing IBA1 positive cell and green arrow is showing PDIA3 positive cell: C-D) Percentage of microglia cells PDIA3 expressing (Panel C) and percentage of PDIA3 positive cells (Panel D) in GBM specimens. * $p<0.05$; ** $p<0.002$.

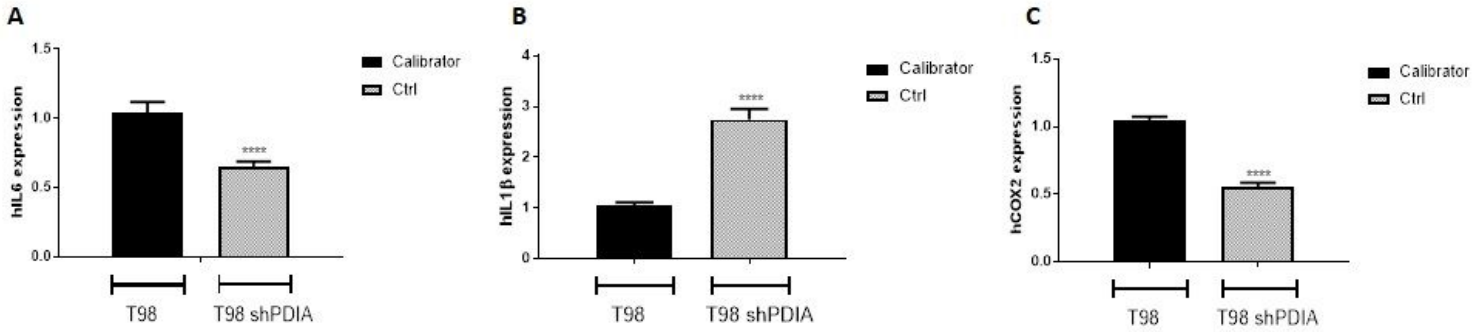

Figure 3

Figure 3

Effects of PDIA3 silencing on T98G: Data shows basal expression of IL6, IL1β and COX2 gene compared to calibrator. **** p<0.0001.

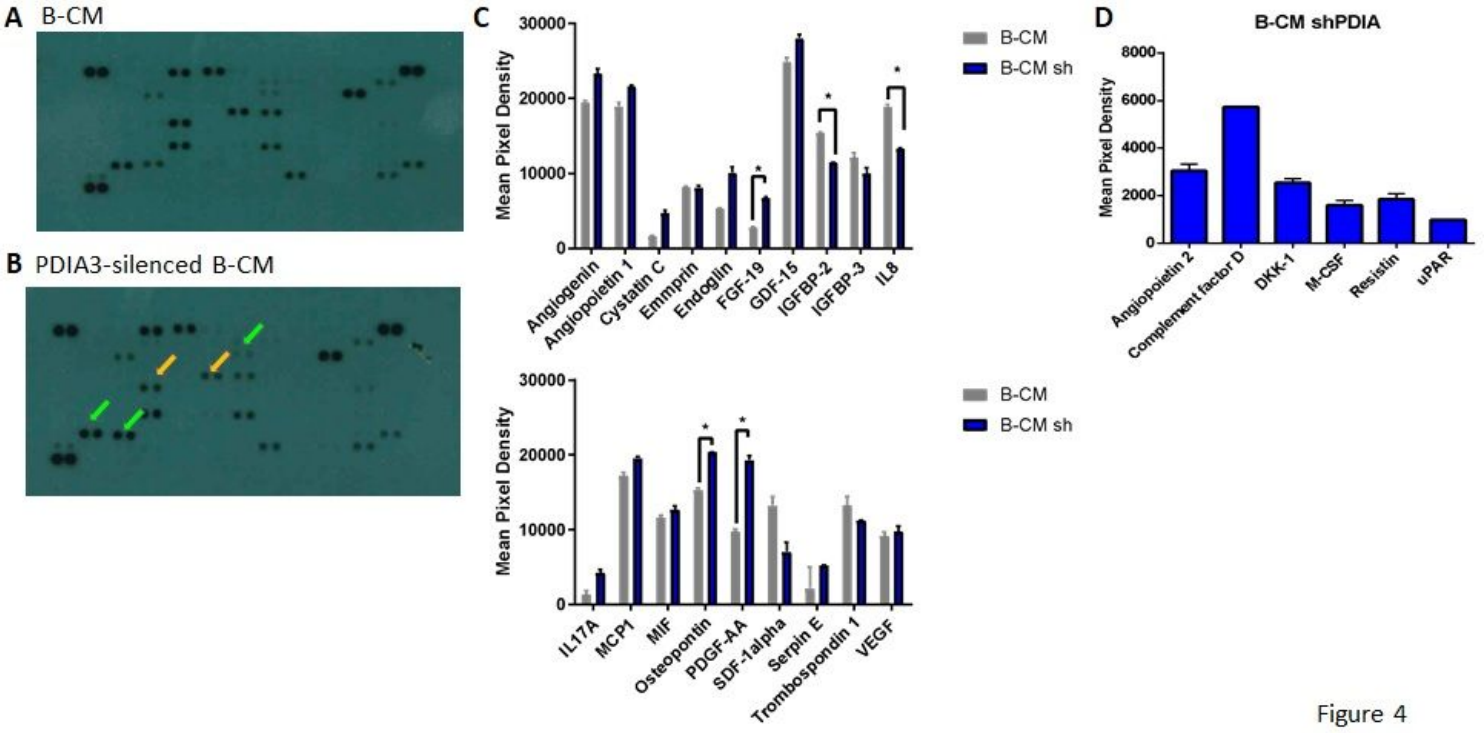

Figure 4

Figure 4

Release of cytokines and chemokines cell culture media of glioma cells. A) B-CM; B) PDIA3-silenced B-CM; C) Semi-quantitative analysis of cytokines and chemokines released; D) Cytokines and chemokines expressed only after PDIA3 silencing. Yellow arrow: down-regulated cytokines and chemochines; Green Arrow: up-regulated cytokines and chemokines. * p<0.05.

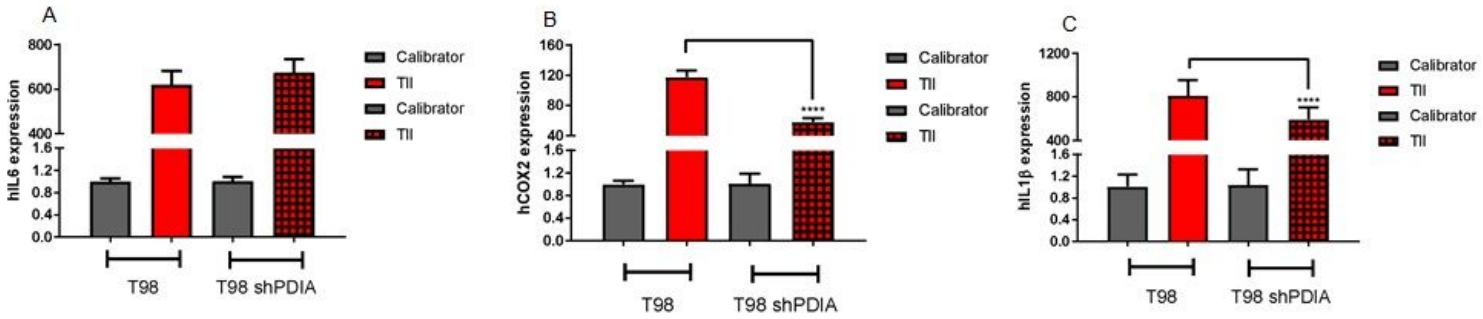

Figure 5

Figure 5

Effects of PDIA3 silencing on IL6, IL1β and COX2 gene expression: Cells were treated with TII for 8 hours. Data are compared to calibrator. * p<0.05; **** p<0.0001.

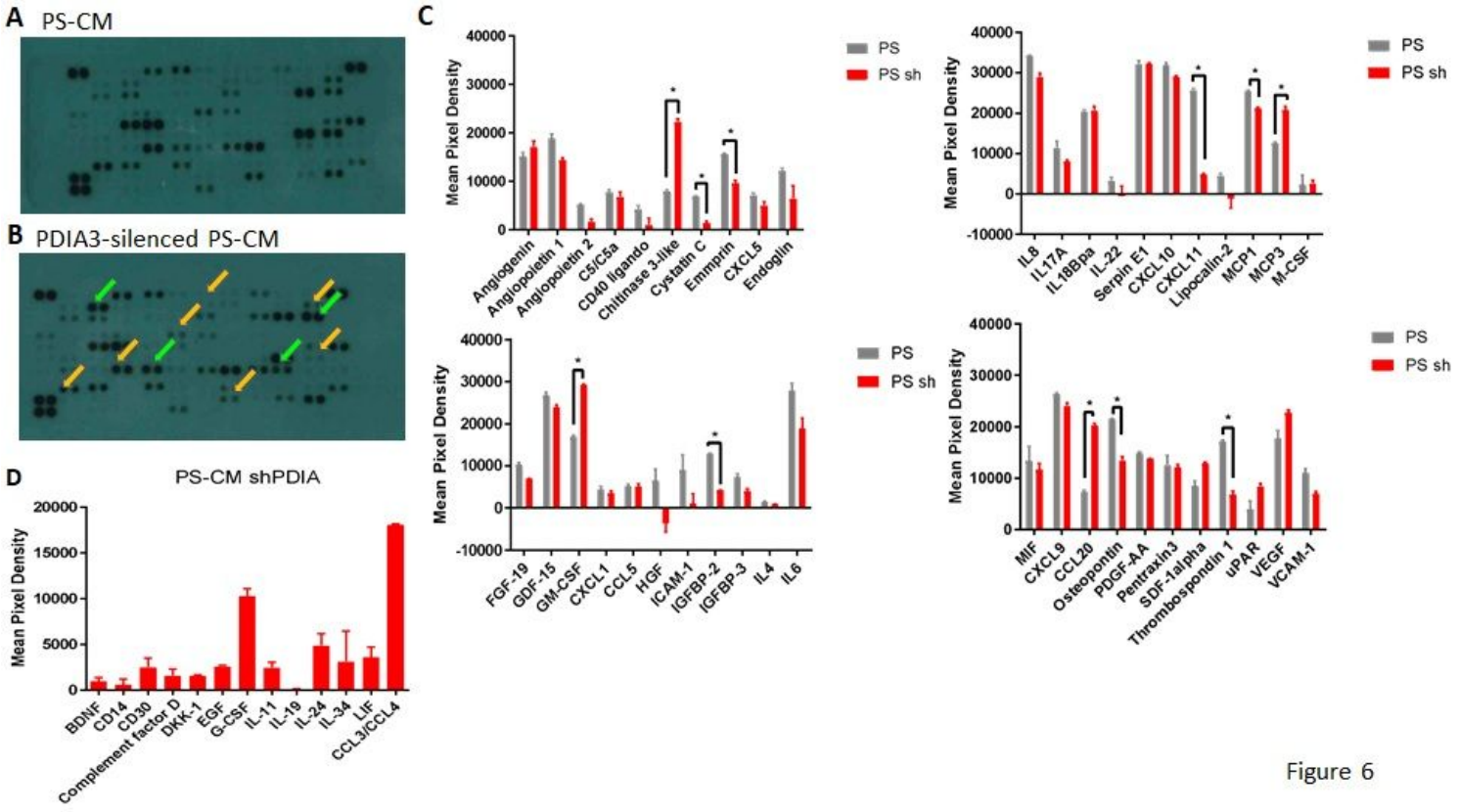

Figure 6

Figure 6

Release of cytokines and chemokines cell culture media of glioma cells. A) PS-CM; B) PDIA3-silenced PS-CM; C) Semi-quantitative analysis of cytokines and chemokines released; D) Cytokines and chemokines expressed only after PDIA3 silencing. Yellow arrow: down-regulated cytokines and chemochines; Green Arrow: up-regulated cytokines and chemokines. * $p<0.05$.

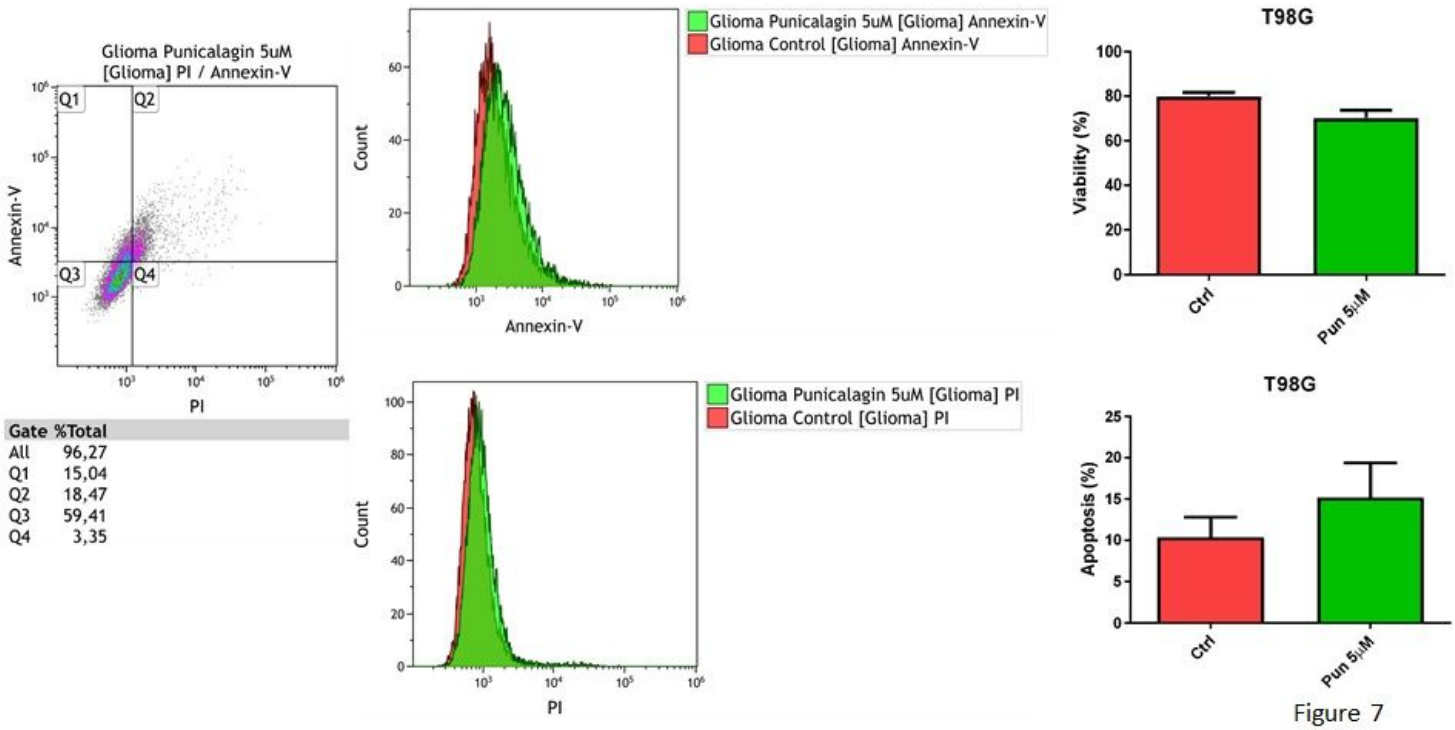

Figure 7

Viability of T98G after Punicalagin challenge: T98G were treated with Punicalagin 5µM for 24 hours.

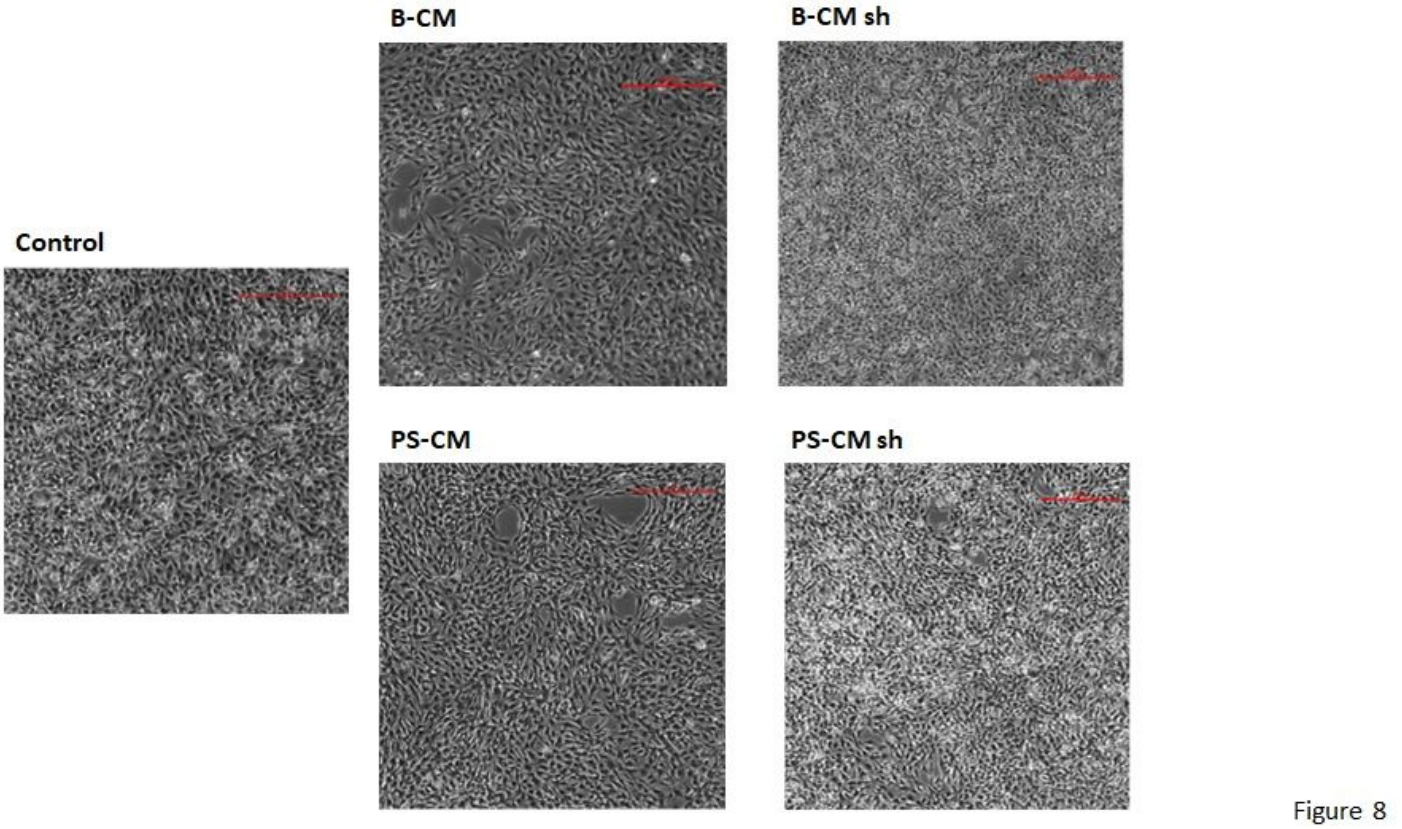

Figure 8

CHME-5 observed by phase-contrast microscopy. Magnitude 10x

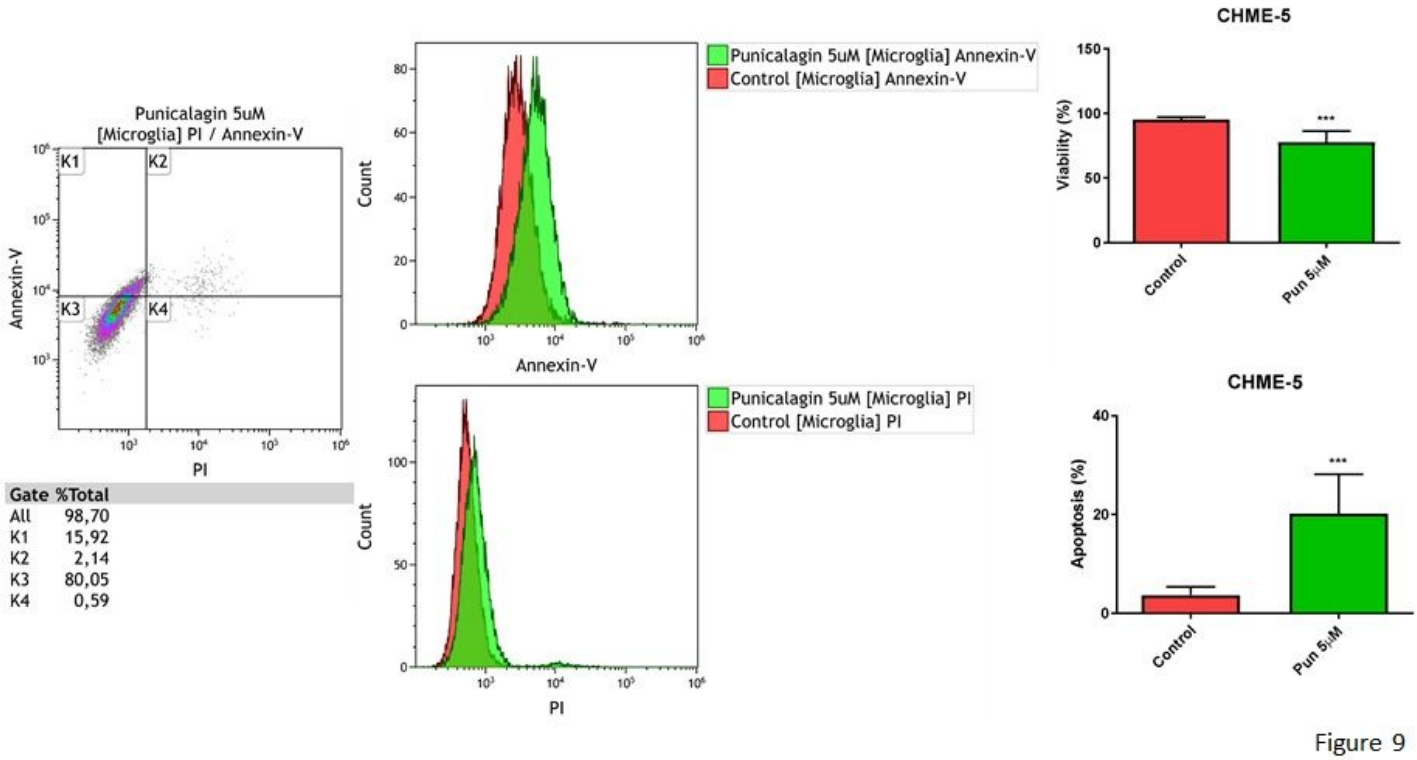

Figure 9

Figure 9

Viability of CHME-5 after Punicalagin challenge: CHME-5 were treated with Punicalagin 5µM for 24 hours. *** p<0.001.

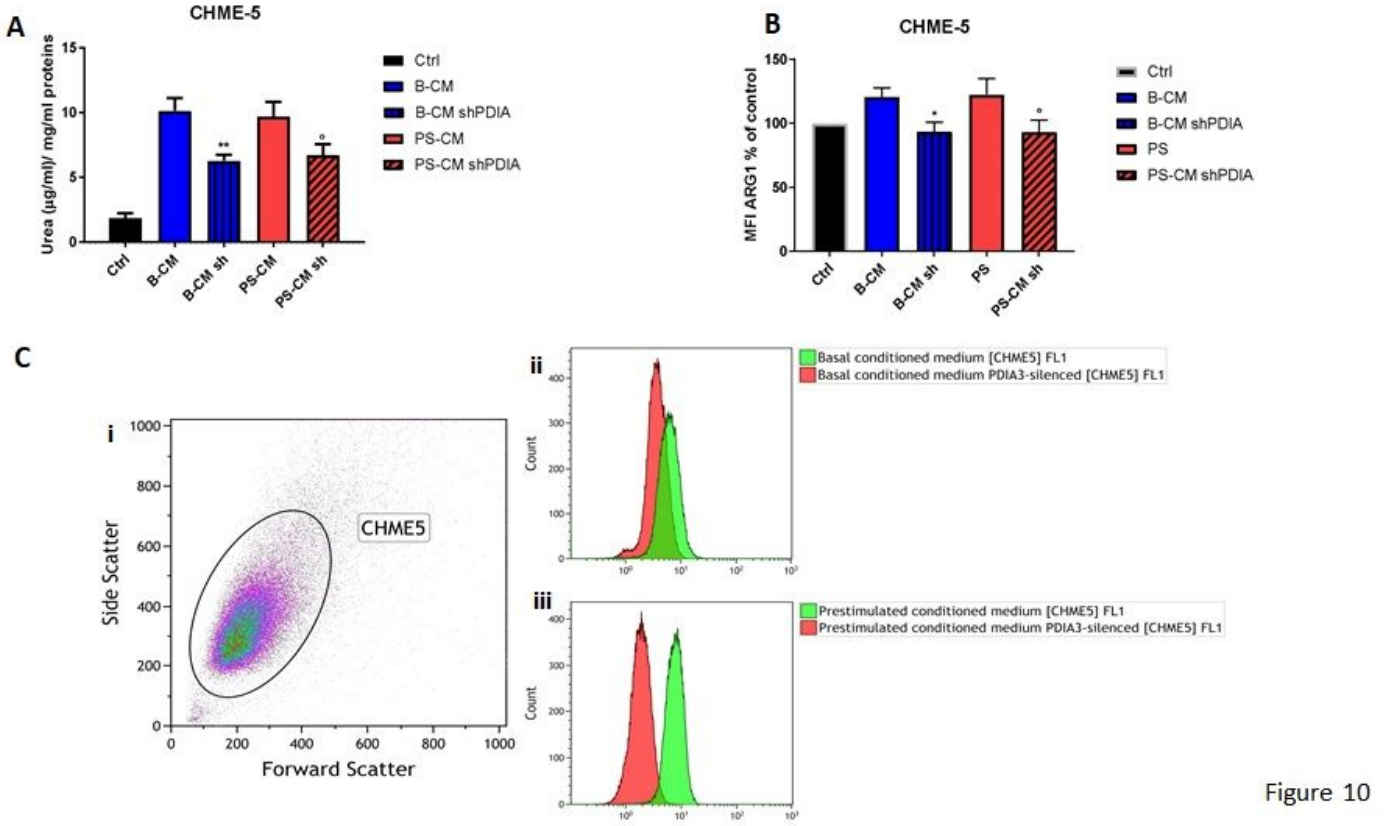

Figure 10

Figure 10

Analysis of M2 phenotype of CHME-5: A) CHME-5 were treated with CMs for 48h; B) Flow cytometry analysis of ARGINASE1: CHME-5 were treated for 24 hours with both CMs from T98G and PDIA3-silenced T98G. Data are shown as percentage of control. C) Flow cytometry: i) Dot plot Forward Scatter (FS) versus Side Scatter (SS). Each dot represents a single cell analyzed by the flow cytometer. The characteristic position of different cell population is determined by differences in cell size and granularity. ii) Fluorescence intensity measurements for Basal conditioned medium. Basal conditioned medium results increased in fluorescence intensity to the right. iii) Fluorescence intensity measurements for Prestimulated conditioned medium. Prestimulated conditioned medium results increased in fluorescence intensity to the right. * $p<0.05$; ° $p<0.05$; ** $p<0.002$.

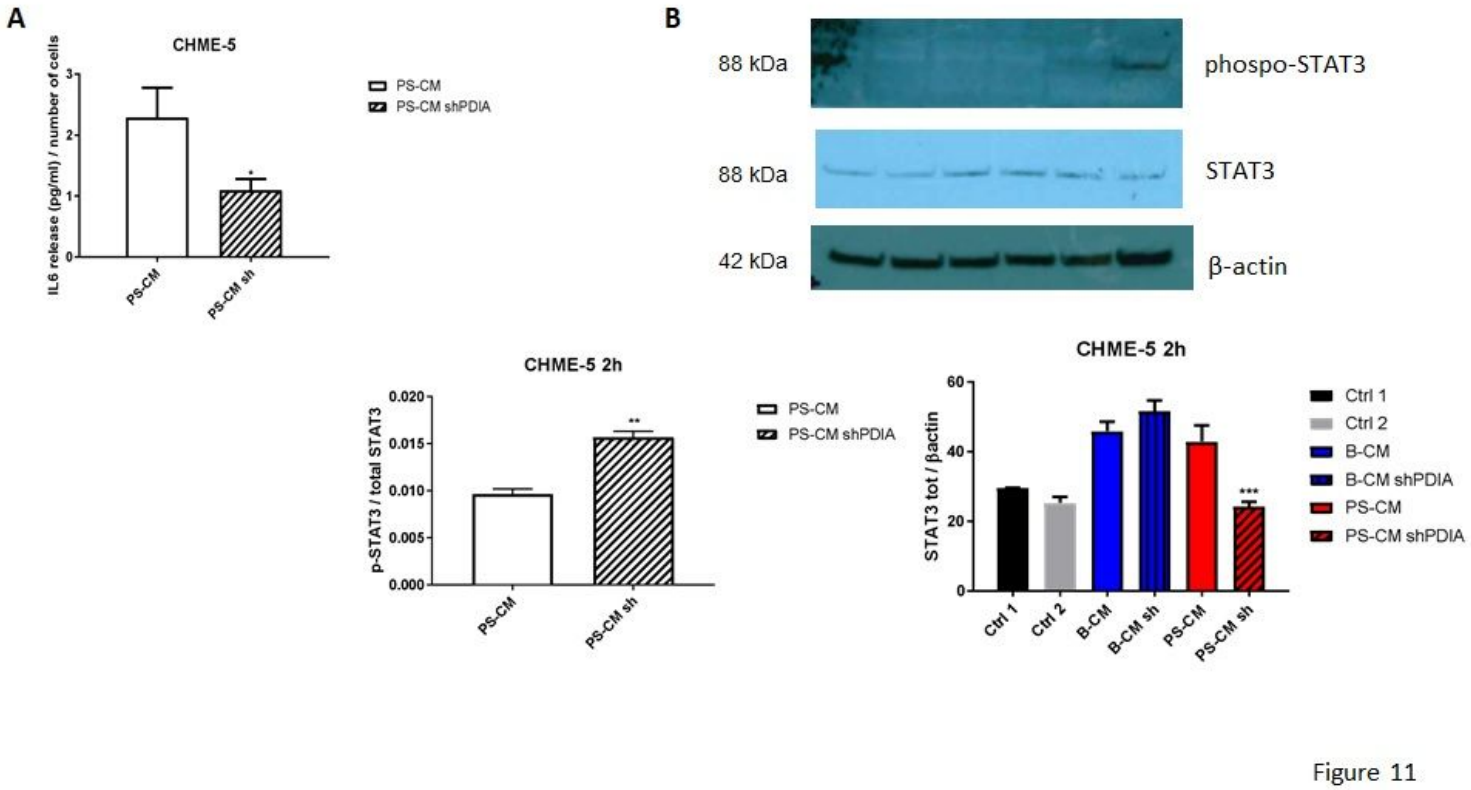

Figure 11

Figure 11

Effects of CMs on CHME-5 considering IL6 release: A) CHME-5 were treated with CMs for 24h. B-CMs shows no effect (data not shown); B) Evaluation of p-STAT3 and STAT3 expression in microglia-glioma interaction: CHME5 were treated for 2 hours with CMs from T98G and with CMs from PDIA3-silenced T98G. Treatments: control 1, control 2, B-CM, PDIA3-silenced B-CM, PS-CM, PDIA3-silenced PS-CM. * $p<0.05$; ** $p<0.002$; *** $p<0.0002$.

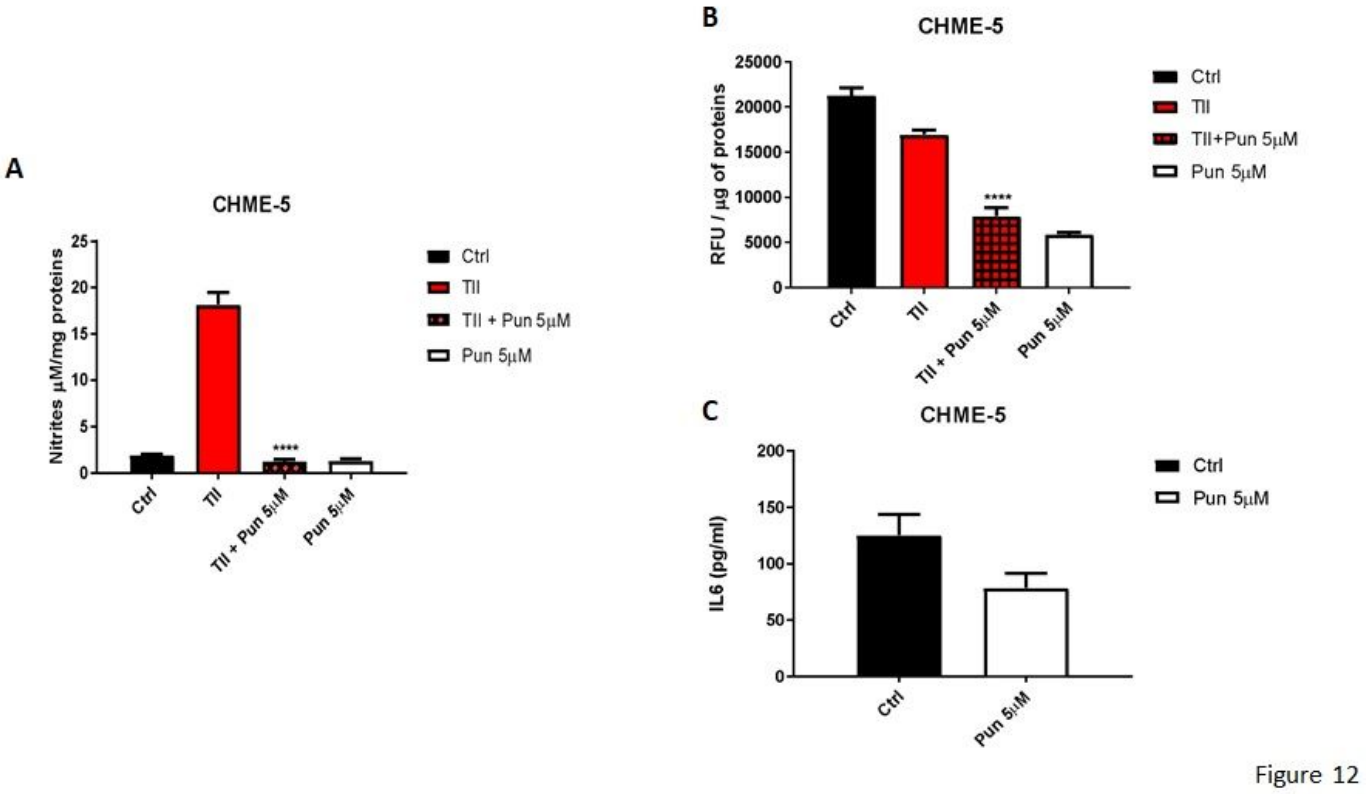

Figure 12

Figure 12

Anti-inflammatory properties of Punicalagin on CHME-5. A) CHME-5 treated for 48 hours with proinflammatory cytokines mix (TII) alone and in association with Punicalagin; B) IL6 release after 24 hours of treatment with Punicalagin; C) DCF production after 48 hours of treatment with TII alone and in association with Punicalagin. **** $p<0.0001$.

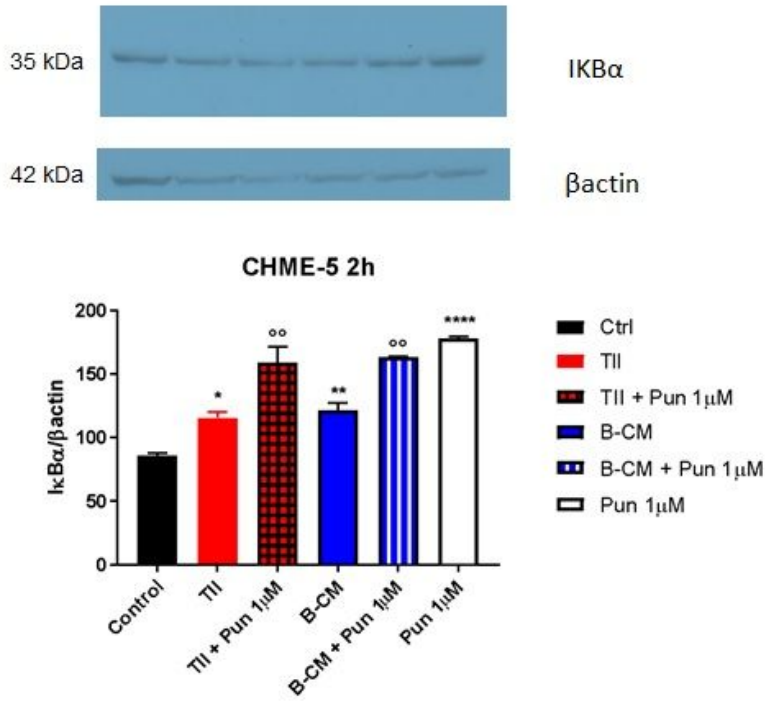

Figure 13

Figure 13

Evaluation of IκBα expression after Punicalagin challenge: CHME-5 were treated with different stimuli for 2 hours. TII, B-CM and Punicalagin are compared to control, TII+Pun, B-CM+Pun are compared to the same treatment given alone.* p<0.05; **, °° p<0.002; **** p<0.0001.

Supplementary Files

This is a list of supplementary files associated with this preprint. Click to download.

- Additionalfile3.docx
- Additionalfile3.docx
- Additionalfile2.docx
- Additionalfile2.docx
- Additionalfile1.docx
- Additionalfile1.docx